Femtosecond Population Inversion and Stimulated Emission of Dense Dirac Fermions in Graphene

T. Li,[1] L. Luo,[1] M. Hupalo,[1] J. Zhang,[1,2] M. C. Tringides,[1] J. Schmalian,[1,3] and J. Wang[1]

[1]*Ames Laboratory and Department of Physics and Astronomy, Iowa State University, Ames, Iowa 50011, USA*
[2]*Department of Physics, College of William and Mary, Williamsburg, Virginia 23187, USA*
[3]*Institute for Theory of Condensed Matter and Center for Functional Nanostructures, Karlsruhe Institute of Technology, Karlsruhe 76128, Germany*

We show that strongly photoexcited graphene monolayers with 35 fs pulses *quasi-instantaneously* build up a broadband, inverted Dirac fermion population. Optical gain emerges and directly manifests itself via a negative conductivity at the near-infrared region for the first 200 fs, where stimulated emission completely compensates absorption loss in the graphene layer. Our experiment-theory comparison with two distinct electron and hole chemical potentials reproduce absorption saturation and gain at 40 fs, revealing, particularly, the evolution of the transient state from a hot classical gas to a dense quantum fluid with increasing the photoexcitation.

Graphene is gradually emerging as a prominent platform for ultrafast photonics and optoelectronics [1–3]. Growing evidence was demonstrated in, e.g., broadband transparency and universal absorption from the near-infrared to visible [4], carrier dynamics [5], saturable absorption [6], pulsed photoluminescence [7–9], and coherently driven photo-currents [10]. For graphene to play a significant role in ultrafast laser technology or telecommunications that exceed semiconductor nanostructure performance, it is vital to investigate femtosecond nonlinearities of strongly photoexcited states. Prior time-resolved studies in graphene have been mostly concerned with the weak excitation regime where the photoexcited carrier density is much smaller than the initial background carrier density. In this case a linear power dependence of transient signals was observed [5,11–13].

Ultrafast photoexcitations strongly alter the thermodynamic equilibrium of electronic states and lead to a series of temporally overlapping rapid processes in graphene, as illustrated in Fig. 1(a). First, during or immediately following the pulse duration τ_p, photoexcitations are *coherent*. Then, electron-electron collisions lead to decoherence and eventually to a quasithermal transient distribution after a time τ_{th}. Finally, for longer times via coupling to phonons, the system relaxes back to equilibrium via cooling of hot carriers (τ_c) and recombination of electron-hole pairs (τ_r). In most semiconductors and their nanostructures, where $\tau_{th} \gg \tau_p$ for ~10 fs laser pulses [14], ultrafast nonlinear photoexcitations lead to a largely nonthermal, peaked distribution close to the pump photon energy and *state filling* dominates on the 10 s of fs time scale [first panel, Fig. 1(b)].

In this Letter, we demonstrate that graphene is in the opposite limit $\tau_{th} < \tau_p$ for 35 fs pulses, where a broadband quasiequilibrium, yet population inverted dense Fermi

system emerges during the pulse propagation. The photoexcited phase space is quickly depleted via carrier-carrier collisions, leading to *band filling* [second panel of Fig. 1(b)]. Most intriguingly, we demonstrate that broadband gain emerges below the excitation photon energy via stimulated emission. The broadband optical gain directly
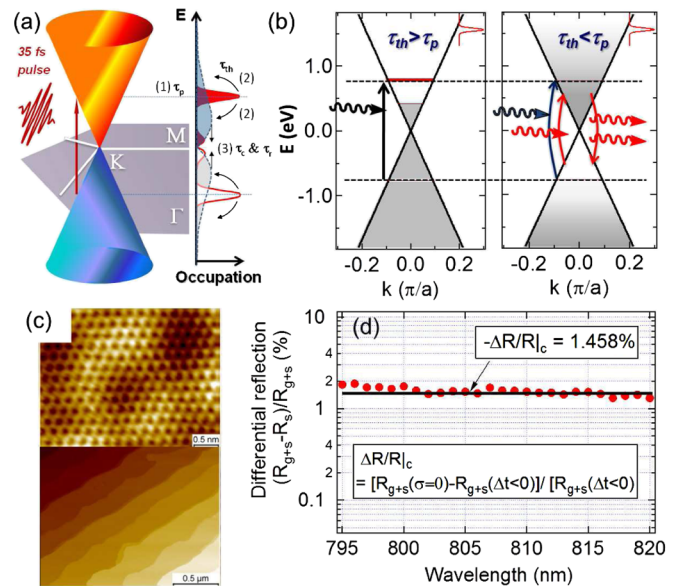

FIG. 1 (color online). (a) Schematics of ultrafast optical interband excitations. (b) Dispersion of our electron-doped graphene monolayers ($\mu = 0.4$ eV) illustrating state filling (left) and band filling (right) that leads to stimulated emission from a broadband, inverted population (red arrow). Also shown together is the pump pulse spectrum. (c) STM images of tomography of the sample used. (d) The static differential reflectivity spectra (red dots). The threshold $\Delta R/R_c$ for zero conductivity can be directly determined ~ − 1.46% (black line, see text for details).

manifests itself via a remarkable negative conductivity at the near-infrared probe energy detuning even ~400 meV below the excitation level within hundreds of fs. The transient states can be quantitatively described in terms of distinct electron and hole chemical potentials, which evolve from a hot classical gas to a dense quantum fluid with increasing the excitation from the linear to the highly nonlinear regime. Such femtosecond build-up of high-density and broadband population inversion has implications in advancing gaphene-based above-terahertz speed modulators, saturable absorbers and gain mediums.

A Ti:sapphire amplifier with central wavelength 800 nm ($\hbar\omega = 1.55$ eV) and $\tau_p = 35$ fs is used to pump an optical parametric amplifier (900–2400 nm) to produce near-infrared probes below the 1.55 eV excitation. Ultrafast degenerate and nondegenerate differential reflectivity changes $\Delta R/R$ with ~40 fs time resolution are recorded with tunable pump fluences, which exhibits no pump polarization dependence. Our epitaxial graphene monolayer sample was grown by thermal annealing in ultrahigh vacuum on a Si-terminated 6H-SiC(0001). The Fermi energy is ~0.4 eV in the sample [Fig. 1(b)] reflecting the substrate-induced electron doping as reported [15,16]. Figure 1(c) shows the STM characterizations of tomography of our samples used, which show homogenous carbon monolayer in atomic length scales (top) and μm scales with smooth overgrowth on the steps of SiC surface (bottom). The strong dependence of the $6\sqrt{3} \times 6\sqrt{3}R30$ reconstruction modulation on the bias voltage confirm the single layer graphene, with the homogeneity of the sample better than 90% across the entire probe region. The

monolayer thickness is further confirmed by the optical deferential reflection spectra [Fig. 1(d)], determined by the measurements with (R_{g+s}) or without (R_s) graphene on SiC substrate.

To understand optical response in graphene, we expand the solution of the Fresnel equation with respect to σ/c (of the order of the fine structure constant of quantum electrodynamics $\alpha_{\text{QED}} = e^2/(\hbar c) \approx 1/137 \ll 1$) and obtain (also see supplemental material [17])

$$\frac{R_{s+g} - R_s}{R_s} = \frac{4}{n_s^2 - 1} \frac{4\pi}{c} \sigma'(\omega) + O(\alpha_{\text{QED}}^2). \quad (1)$$

$\sigma'(\omega) = \text{Re}\sigma(\omega)$ is the real part of the complex optical conductivity. Equation (1) leads to two key aspects: (i) the reflection coefficient provides a direct measurement $\sigma'(\omega)$ (or absorption) without reference to any model assumption, e.g., $\Delta R/R = 16\pi/(n_s^2 - 1)c(\sigma'(\tau) - \sigma'(0))$; (ii) using the established universal value $\sigma_0 = \frac{e^2}{4\hbar}$ for graphene monolayer without pulse [2,3], there exists a threshold value for the photoinduced differential reflectivity that corresponds to the transition to a negative optical conductivity and thus to gain behavior $\Delta R/R|_c = -\frac{4\pi\alpha_{\text{QED}}}{n_s^2 - 1}$. With $n_s = 2.7$ for SiC substrate follows $\Delta R/R|_c = -1.4582\%$., which can be determined experimentally by measuring the optical spectra [Fig. 1(d)]. Here the reflection from the zero conductivity state in the pumped graphene/SiC sample exactly corresponds to the case of bare SiC substrate. It is also critical to note that the negative $\sigma'(\omega)$ represents the hallmark for the existence of gain in the excited *graphene*
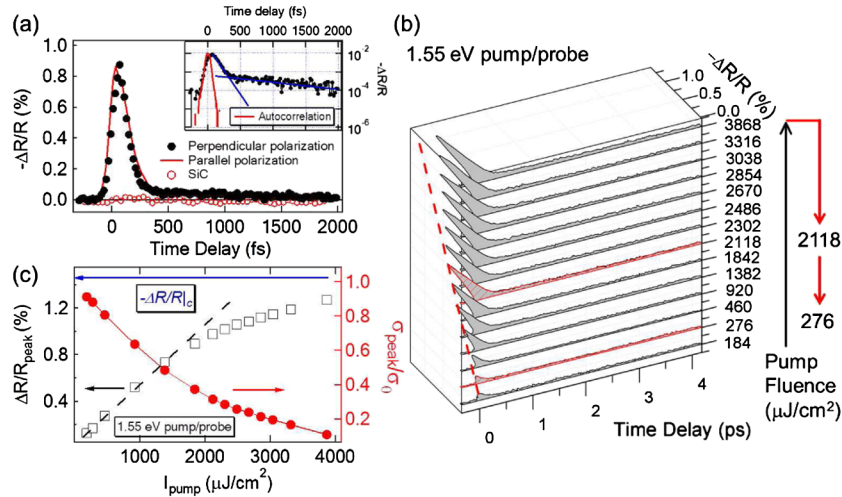

FIG. 2 (color online). (a) The degenerate differential reflectivity at 1.55 eV for the graphene monolayer (solid dots and line) and SiC substract (empty dots) under the pump fluence of 1842 μJ/cm^2. Inset: $\Delta R/R$ in logarithmic scale (black dots) together with the pump-probe autocorrelation (red line). (b) $\Delta R/R$ at 1.55 eV for different pump fluences. The dashed straight line is a guide for the eyes. The different curves were taken in the order as marked. The perfect overlap of the pair of curves indicates the signals are not caused by laser-induced permanent changes. (c) The peak $\frac{\Delta R}{R}|_{\text{peak}}$ as function of the pump fluence (black squares) and the corresponding conductivity (red solid dots). Blue arrow marks the threshold for zero conductivity $\Delta R/R|_c = -1.4582\%$ (see text). Dashed line: linear dependence (guide to the eyes).

layer, which should not be confused with the reflection loss in the substrate.

Next we present ultrafast degenerate reflectivity spectroscopy to reveal femtosecond nonlinear saturation. A typical temporal profile of $\Delta R/R$ at 1.55 eV in the graphene monolayer (black dots) is shown in Fig. 2(a), clearly showing a negative transient signal. Note the photoinduced change is negligible in the controlled experiment using the SiC substrate without graphene (red circles). Several temporal regimes can be identified in the logarithmic scale plot in the inset: a pulse width limited rise ∼40 fs (red line), followed by a biexponential decay of 70 fs and 2.5 ps (blue lines). The power dependence of photoinduced $\Delta R/R$ at the maximum of ΔR in Fig. 2(b) reveals a clear nonlinear behavior. Figure 2(c) summarizes $\Delta R/R$ at the signal peak for different pump fluences I_p, showing a nonlinear pump fluence dependence above $\simeq 1850$ $\mu J/cm^2$, at least 1 order of magnitude higher than what is reported for semiconducting single-walled carbon nanotubes [18]. Following Eq. (1), the measured $\Delta R/R$ allows us to obtain the corresponding peak conductivity in photoexcited graphene, as shown by the red dot in Fig. 2(c) (normalized by σ_0). At the highest pump fluence used $\simeq 3868$ $\mu J/cm^2$, $\Delta R/R$ peak approaches 90% of the critical value $\Delta R/R|_c$ and the peak conductivity drops to only 10% of σ_0.

The most striking response is obtained after ultrafast *nondegenerated* differential reflectivity. Figure 3(a) shows dynamics using 1.55 eV pump and low energy probes at 1.16 and 1.33 eV. It is clearly visible that, at high pump fluence, the critical value $\Delta R/R|_c$, the threshold for negative conductivity (blue lines), indeed occurs for both cases. With increasing pump fluence, Fig. 3(b) indicates that, above $I_{pump,c} \simeq 2000$ $\mu J/cm^2$, the stimulated infrared emission surpasses absorption loss in the photoexcited graphene for the 1.16 eV probe. The temporal profiles for pump fluence above the gain threshold indicate that the negative conductivity can persist for hundreds of fs, e.g., the 3960 $\mu J/cm^2$ at 1.16 eV. We emphasize three key aspects of this conclusion: (i) the critical value has not been reached by the degenerate pump or probe [Fig. 2(c)] and appears exclusively for nondegenerate condition when probing below 1.55 eV, (ii) the $\Delta R/R|_c$ is a *model independent value* that corresponds to $\sigma = 0$, which directly indicates the transition from loss to gain behavior, (iii) the femtosecond emergence of stimulated emission even at the ∼400 meV below the excitation level indicates very rapid establishment of broadband population inversion and broadband gain in the strongly photoexcited graphene states.

We can extract the number of photoexcited electrons in graphene immediately after the laser pulse from

$$n_{ex}(I_p) = \int_{-\infty}^{\infty} \frac{dt}{\tau_p} n_{ex}(t, I_p) = \frac{1}{\hbar\omega} \int_{-\infty}^{\infty} \frac{dt}{\tau_p} I(t, I_p) A(t), \quad (2)$$
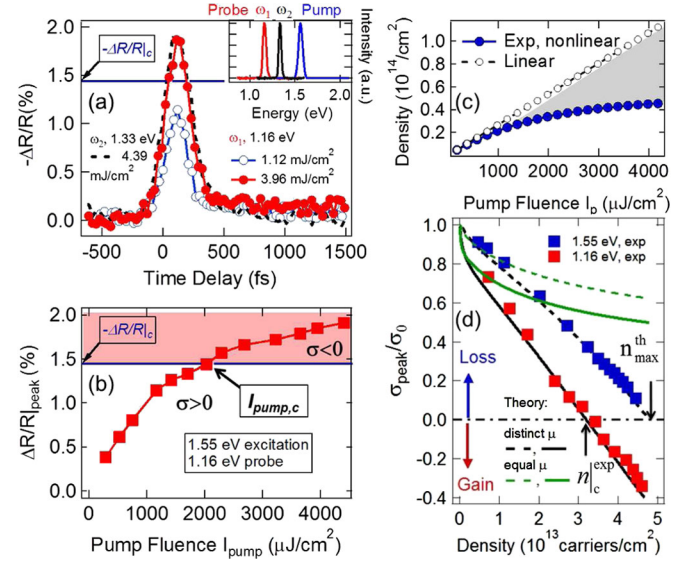

FIG. 3 (color online). (a) Ultrafast $\Delta R/R$ at 1.55 eV pump, 1.16 eV probe, at 1116 and 3960 $\mu J/cm^2$, and 1.33 eV probe, at 4390 $\mu J/cm^2$, respectively. Blue arrow marks $\Delta R/R|_c = -1.4582\%$ for zero conductivity. Shown together are the pump and probe spectra. (b), The peak transient reflectivity as function of the pump fluence. (c), The extracted transient fermion density at 40 fs (blue dots), as explained in the text, which is significantly lower than $A_0 I_p/\hbar\omega$ obtained from the universal conductivity (open circles), as illustrated in shadow area. (d), Theory (lines) vs experimental values (rectangles) for nondegenerate (red) and degenerate (blue) transient conductivity at 40 fs. Shown together (lines) are two model simulations with the single (green) or distinct (black) chemical potentials.

where $I(t, I_p)$ is the Gaussian pulse envelop $I(t, I_p) = I_p \sqrt{\frac{4\ln 2}{\pi}} \exp[\frac{-4\ln 2}{\tau_p^2} t^2]$, normalized such that the total pulse fluence is $I_p = \int_{-\infty}^{\infty} \frac{dt}{\tau_p} I(t, I_p)$. For $\tau_{th} \ll \tau_p$, the absorption coefficient $A(t)$ is determined by the adiabatic dependence of the absorption on the pump fluence and can be derived from the measured saturation curve at 40 fs [Fig. 2(c)] by $A(t) = A_0 + \Delta A(t) = A_0(1 + \frac{\Delta A(t)}{A_0})$ (see supplemental material [17]). Without pump, the absorption of a graphene monolayer on SiC is $A_0 = \frac{4}{(1+n_{SiC})^2} \frac{\pi e^2}{\hbar c}$. Using the actual absorption $A(t)$, instead of A_0, is crucial as the linear relation $\hbar\omega n_{ex} \simeq A_0 I_p$ substantially overestimates n_{ex} during the pulse propagation, as shown in Fig. 3(c). From Eq. (3), we extract from the data extremely dense photoexcited fermions $n_{max}^{exp} \simeq 0.5 \times 10^{14}$ cm^{-2} for our electron-doped sample, surpassing the saturation in a 10 nm GaAs quantum well by more than 2 orders of magnitude under the similar excitation condition [19].

Next we analyze the transient state at $\tau_{th} < t < \tau_c$. Immediately after the pulse at $\Delta t = 40$ fs, energy of the electronic system is conserved because no relaxation into the phonon system has taken place yet. In the case of highly excited graphene, the phase space constraint of the Dirac

spectrum leads to an approximate conservation of numbers of photoexcited holes and electrons, valid to the second order in the electron-electron Coulomb interaction [20,21]. A recent explicit analysis of the short time dynamics by Winzer *et al.* indicates that the conservation of hole and electron numbers is a good approximation for the high excitation regime [22]. Consequently, this gives rise to a slow imbalance relaxation and thus to a population inverted transient state with quasiconserved occupations of the two branches of the Dirac cone in our experimental condition. These, together with the assumption that a de-cohered, quasithermal state leads to the nonequilibrium transient distribution function ($\varepsilon = \upsilon p$):

$$f_{e(h)}(\varepsilon) = \frac{1}{\exp(\frac{\varepsilon - \mu_{e(h)}}{k_B T_e}) + 1}, \tag{3}$$

characterized by the electron temperature, T_e and two *distinct* chemical potentials μ_e and μ_h, for electrons in the upper and holes in the lower branch of the spectrum, respectively. Note that a scenario based on a single chemical potential does not explain the demonstrated population inversion. In thermodynamic equilibrium holds $\mu_e = -\mu_h = \mu$ and $T_e = T$. In general, T_e and $\mu_{e(h)}$ are functions of given photon energy, $\hbar\omega$, total density, and density of photoexcited carriers, n_{ex} (see supplemental section [17]). The nonequilibrium optical conductivity is calculated in Keldysh formalism [23] and follows as

$$\sigma(\omega) = \frac{e^2}{4\hbar}(1 - f_e(\hbar\omega/2) - f_h(\hbar\omega/2)). \tag{4}$$

Figure 3(d) compares the peak transient conductivity with the calculated conductivity $\sigma(\omega)$ of Eq. (4) as function of n_{ex} for two probe photon energies 1.55 and 1.16 eV. Excellent agreement between experiment and theory is found which demonstrates the faithful representation of the transient state at 40 fs by the distribution function, Eq. (3). For the degenerate scheme, our theory (black dashed line) yields $\sigma \to 0$ and thus perfect transparency for $n_{\text{max}}^{\text{th}} = 0.48 \times 10^{14}$ cm^{-2}. Once the system is driven

into this regime, a balance between stimulated emission and absorption will lead to the perfect transparency. For the nondegenerate scheme, by probing at 1.16 eV, our theory (black solid line) predicts a critical density $n|_c^{\text{th}} = 0.32 \times 10^{14}$ cm^{-2} for the transition from loss to gain. All of these results agree quantitatively with the experimental values $n_{\text{max}}^{\text{exp}} = 0.5 \times 10^{14}$ cm^{-2} and $n|_c^{\text{exp}} = 0.34 \times 10^{14}$ cm^{-2}, respectively, (black arrows) [24]. In addition, the experiment-theory comparison of the conductivity $\frac{\sigma(\omega)}{\sigma_0}$ is shown in Fig. 3(d) for the distinct- (black lines) and the equal-chemical-potential model (green lines) at the probe photon energy $\hbar\omega = 1.55$ eV and 1.16 eV, which clearly identifies the validity of the distinct-μ model calculation.

The detailed information of the transient state at 40 fs as a function of n_{ex} is shown in Fig. 4(a) for the transient chemical potentials and carrier temperature (inset). For weak excitation $n_{\text{ex}} \ll \omega^2/\upsilon^2$ (but larger than the number of thermally excited carriers before the pulse) we find $k_B T_e \sim \hbar\omega$ while $\mu_h < 0$, corresponding to a hot, dilute gas of classical holes. Increasing n_{ex} changes the sign of the hole chemical potential ($\mu_h > 0$) and eventually decreases T_e, i.e., as a function of pump fluence we enforce a crossover from a hot and dilute Maxwell-Boltzmann gas to a degenerate population inverted quantum system, with $\mu_e + \mu_h$ measuring the degree of population inversion [25]. Most notably, the transient conductivity, $\sigma(\omega)$, of Eq. (4) changes sign if $\mu_e + \mu_h$ crosses $\hbar\omega$, with broadband optical gain due to population inversion for the entire region $\omega < \mu_e + \mu_h$ ($\sigma < 0$), as illustrated between two intersection planes in Fig. 4(c). The separation between the planes is shown to approach to the pump energy 1.55 eV at high excitation density, consistent with our experiment.

We have shown the existence of pronounced femtosecond population inversion and near-infrared gain in strongly photoexcited graphene monolayers. These results clearly reveal the transient electron and hole potentials are separated on the time scale of hundreds of fs. Our experimental-theory comparison explains well the absorption saturation
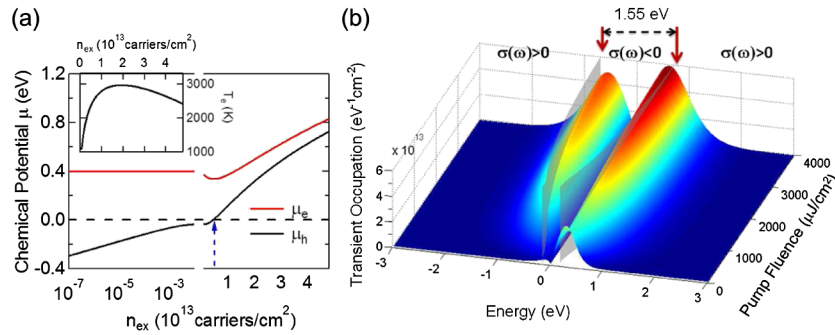

FIG. 4 (color online). (a) The calculated transient electron (μ_e), hole (μ_h) chemical potentials and transient temperature (inset) as function of photoexcited carrier density. (b) Transient electron and hole distribution function at 40 fs are plotted for different pump fluence. The two intersection planes represent the occupation probability of an electron-hole pair at the given excitation photon energy is equal to unity, i.e., $f_e(\omega/2) + f_h(\omega/2) = 1$.

and gain from the dense fermions, and reveals a crossover from a hot Maxwell-Boltzmann gas to a degenerate dense Fermi-Dirac system.

[1] F. Bonaccorso *et al.*, Nature Photon. **4**, 611 (2010).
[2] A. H. Castro Neto *et al.*, Rev. Mod. Phys. **81**, 109 (2009).
[3] Kin Fai Mak *et al.*, Phys. Rev. Lett. **101**, 196405 (2008).
[4] R.-R. Nair *et al.*, Science **320**, 1308 (2008).
[5] J.-M. Dawlaty *et al.*, Appl. Phys. Lett. **92**, 042116 (2008); P.-A. George *et al.*, Nano Lett. **8**, 4248 (2008); H. Choi *et al.*, Appl. Phys. Lett. **94**, 172102 (2009).
[6] Z. Sun *et al.*, ACS Nano **4**, 803 (2010); Q. Bao *et al.*, Adv. Funct. Mater. **19**, 3077 (2009).
[7] R.-J. Stöhr *et al.*, Phys. Rev. B **82**, 121408 (2010).
[8] C.-H. Liu *et al.*, Phys. Rev. Lett. **105**, 127404 (2010).
[9] W. Lui *et al.*, Phys. Rev. B **82**, 081408 (2010).
[10] D. Sun *et al.*, Nano Lett. **10**, 1293 (2010).
[11] M. Breusing, C. Ropers, and T. Elsaesser, Phys. Rev. Lett. **102**, 086809 (2009).
[12] R.-W. Newson *et al.*, Opt. Express **17**, 2326 (2009).
[13] D. Sun *et al.*, Phys. Rev. Lett. **101**, 157402 (2008).
[14] J.-L. Oudar *et al.*, Phys. Rev. Lett. **55**, 2074 (1985).
[15] I. Gierz *et al.*, Nano Lett. **8**, 4603 (2008).
[16] M. Hupalo, E. H. Conrad, and M. C. Tringides, Phys. Rev. B **80**, 041401(R) (2009).
[17] See Supplemental Material at http://link.aps.org/supplemental/10.1103/PhysRevLett.108.167401 for details.
[18] J. Wang *et al.*, Phys. Rev. Lett. **104**, 177401 (2010).
[19] D. S. Chemla *et al.*, IEEE J. Quantum Electron. **20**, 265 (1984).
[20] L. Fritz *et al.*, Phys. Rev. B **78**, 085416 (2008).
[21] M. S. Foster and I. L. Aleiner, Phys. Rev. B **79**, 085415 (2009).
[22] Torben Winzer *et al.*, Nano Lett. **10**, 4839 (2010)
[23] L. V. Keldysh, Sov. Phys. JETP **20**, 1018 (1965).
[24] This extremely good agreement between theory and experiment clearly corroborates $\tau_{th} < 40$ fs ($\tau_{th} < \tau_p < \tau_c$). The 70 fs and 2.5 ps relaxation components in Fig. 2(a) can then be naturally assigned to the cooling of hot carriers τ_c and recombination of electron-hole pairs τ_r.
[25] Our analysis for the low photoexcited carrier density and longer, ps relaxation are consistent with the behaviors found in [26]
[26] R. Kim, V. Perebeinos, and P. Avouris, Phys. Rev. B **84**, 075449 (2011)